

New Collision Theory of Cathode Sputtering of Metals at Low Ion Energies

ERICH B. HENSCHKE

Electronic Components Laboratory, Wright Air Development Center, Air Research and Development Command, United States Air Force, Dayton, Ohio

(Received May 14, 1956; revised manuscript received November 20, 1956)

Cathode sputtering is conceived as being produced by purely mechanical collisions between the impinging ions and surface atoms of the target. Energy is lost during the collisions by excitation of Debye waves in the lattice. The collisions are assumed to occur as between perfectly elastic spheres with radii determined by the largest closed electronic shells of the ion and the target atom. Only upper surface atoms of the target can be sputtered; the ejection requires that the momentum transferred to an upper surface atom have a component in normal outward direction and the transferred energy be larger than its binding energy to the lattice, which is assumed to equal the heat of vaporization. With the introduction of a dissipation coefficient, which determines the energy loss during the collision, formulas for the threshold energies at oblique and normal ion incidence and a sputtering rate formula for normal ion incidence at low ion energy have been derived. Experimental data on sputtering are in agreement with the derived formulas. From the derivation of the sputtering rate formula it can be concluded that the threshold energies must be roughly proportional to the squares of the collision radii of the target atoms. This implies a periodicity of the threshold energies within the periods of the periodic system, which has been evidenced by plotting experimental data on threshold energies for 26 metals *versus* atomic number.

1. INTRODUCTION

THE newer experimental results on cathode sputtering such as phenomena at oblique ion incidence, data on threshold energies, and deposit patterns from sputtering single-crystal planes, as obtained by Wehner,¹⁻⁴ are generally strongly in favor of the impulse transfer concept, as initiated by Stark⁵ and developed by Kingdon and Langmuir.⁶ However, a detailed theory treating all the phenomena observed at low ion energy with the same basic principle has not yet been developed. Kingdon and Langmuir⁶ assumed that "two successive impacts on the same thorium atom of a thoriated tungsten filament are necessary for sputtering; the first impact depresses the atom from the surface, while at the second impact the ion is reflected from this depressed atom and knocks off one of the surrounding thorium atoms," provided the energy transferred in this last collision "is greater than the atomic heat of vaporization." For a first approximation the collisions are treated by these authors as perfectly elastic head-on collisions between a free ion with mass m and a free atom with mass M at rest before the collision. The momentum and energy equations for the two consecutive collisions led to the formula

$$E_{\min} = \Delta H_{298} \times \frac{(m+M)^2}{mM} \times \frac{(m+M)^2}{(m-M)^2}, \quad (1.1)$$

where ΔH_{298} is the heat of vaporization at 298° K in ev and E_{\min} the threshold energy in ev. The values of E_{\min} from this formula, if m and M are approximately

equal, are much too high and do not agree with the experimental results.

Sputtering rate formulas, derived from a purely mechanical collision concept, do not exist in the literature.

2. BASIC FEATURES OF THE NEW COLLISION THEORY

In single-crystal or polycrystalline metal surfaces, regardless of the lattice orientation of the crystal plane or of the individual grains, there are always "upper" surface atoms in an outermost plane, designated by M_U in Fig. 1, and "lower" surface atoms in a parallel first or even second lower plane, designated by M_L in Fig. 1. These surface atoms are equally accessible to the perpendicularly impinging ions of mass m , if the assumption is made that the effective collision spheres are the largest closed electronic shells of ion and target atom, thus being considerably smaller than their atomic or even ionic radii. With this assumption in mind, the final step in each sputtering process at any angle of incidence of the ion can be generally described as a collision of the ion with an upper surface atom, in which this atom is hit on its inside hemisphere, so as to obtain an impulse with a component in the direction of the outward normal to the surface. If the energy transferred in this direction to this target atom by the impact of the ion is equal to or greater than the heat of vaporization, with which the atom is assumed to be bound to the crystal lattice plane, then this atom is ejected in the collision.

Sputtering by a direct single collision of the ion with the inside hemisphere of an upper atom is possible only when the ion hits the surface at an oblique angle of incidence [Fig. 1(a)]. For normal ion incidence, sputtering is produced mostly by a double collision of the ion [Fig. 1(b)]; the ion collides first with a lower

¹ G. Wehner, J. Appl. Phys. **25**, 270 (1954).

² G. Wehner, Phys. Rev. **93**, 633 (1954).

³ G. Wehner, J. Appl. Phys. **26**, 1056 (1955).

⁴ G. Wehner, Phys. Rev. **102**, 690 (1956).

⁵ F. Stark, Z. Electrochem. **15**, 509 (1909).

⁶ K. H. Kingdon and F. Langmuir, Phys. Rev. **22**, 148 (1923).

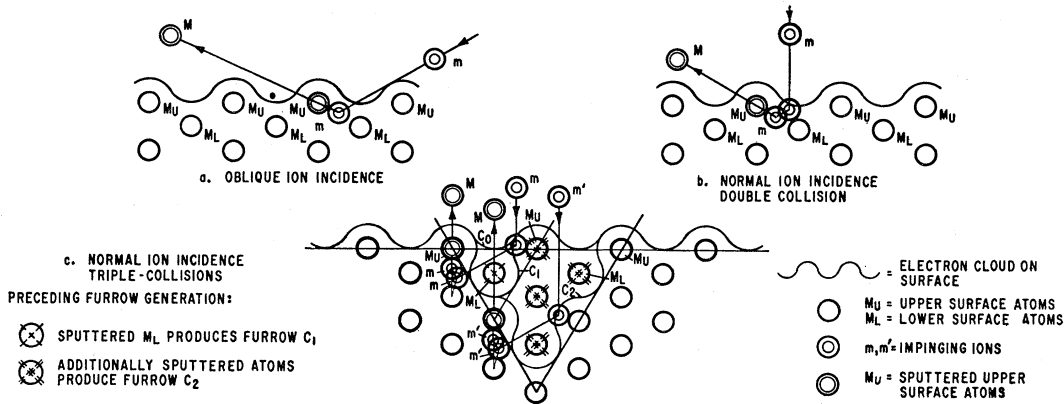


FIG. 1. Different kinds of collision mechanisms in sputtering phenomena.

surface atom and then rebounds and hits an upper surface atom in a second collision on its inside hemisphere. However, from experiments on sputtering of certain single-crystal planes, triple-collision sputtering must also be assumed to occur at normal ion incidence [Fig. 1(c)]. In this case the incident ion is deflected in a first collision with a target atom before it hits a lower surface atom lying perpendicularly under an upper surface atom; in this second collision it rebounds in the direction of the outward normal against the upper atom which is ejected in this third collision.

The collision of the closed shells of ion and target atom may be taken as purely elastic, since the ion velocity is much slower than the velocity of the slowest orbital electron.⁷

Energy losses are due to the fact that the target atom is coupled rather strongly with the atoms of the lattice. Before the moment of highest compression is reached, the ion and the struck atom exchange energy with the neighboring atoms of the lattice. Debye waves are thus excited and dissipated irreversibly into the lattice. The situation is thus similar to that which occurs in the collisions of knocked-on atoms in the theory of radiation damage.⁸

3. MATHEMATICAL TREATMENT OF SPUTTERING COLLISIONS

It will be assumed that the collisions described can be treated with the general principles of classical mechanics, using impulsive forces, in a manner similar to the well-known collisions with restitution.⁹

Two spheres colliding head-on may have the masses

⁷ N. Bohr, Kgl. Danske Videnskab. Selskab, Biol. Medd. **18**, No. 8 (1948).

⁸ F. Seitz and J. S. Koehler, in *Solid State Physics* edited by F. Seitz and D. Turnbull (Academic Press, Inc., New York, 1956), pp. 305-448.

⁹ Reference books on collisions with restitution: E. H. Smart, *Advanced Dynamics* (MacMillan and Company, London, 1951), Vol. 1, p. 165; W. D. MacMillan, *Dynamics of Rigid Bodies* (McGraw-Hill Book Company, Inc., New York, 1946), p. 290; E. F. Routh, *A Treatise on Dynamics of a Particle* (G. E. Stechert & Company, New York, 1898), p. 36.

m and M , the velocities v_0 and V_0 , respectively, before the collision, and the velocities v_1 and V_1 , respectively, after the collision.

From the equation of conservation of momentum,

$$mv_0 + MV_0 = mv_1 + MV_1, \quad (3.1)$$

the relation

$$R = m(v_0 - v_1) = -M(V_0 - V_1), \quad (3.2)$$

expressing the principle of action and reaction of equal magnitude, defines a quantity R which is sometimes called the whole "blow" (Smart⁹) or whole "action" (Routh⁹) between the spheres. From the two Eqs. (3.2), R can be determined as

$$R = \frac{mM}{m+M} [(v_0 - v_1) - (V_0 - V_1)]. \quad (3.3)$$

The impulse of compression R_0 is defined as the impulse acting from the instant of contact of the two spheres to the instant at which the centers of the spheres are closest to each other, which is the moment of greatest compression, i.e., up to the instant when the relative velocity of the spheres is zero, and thus $v_1 = V_1$. The impulse of compression R_0 is therefore, from (3.3),

$$R_0 = \frac{mM}{m+M} (v_0 - V_0). \quad (3.4)$$

For the sputtering collisions of ions and target atoms as described above, the impulse R_0 up to the moment of highest compression of the closed shells, consists of two parts, the impulse R_d used up for the excited Debye waves and the compression impulse R_c for the closed shells.

If a coefficient δ is introduced, so that

$$R_c = \delta R_0, \quad 0 \leq \delta \leq 1, \quad (3.5)$$

the impulse used up in Debye waves would be

$$R_d = R_0(1 - \delta). \quad (3.6)$$

The coefficient δ is an indirect measure of the energy dissipation in the form of Debye waves during the collision and may be called the "dissipation" or "lattice interaction" coefficient. The larger δ is, the smaller is the energy lost in the form of Debye waves.

The whole blow R would therefore consist of the impulse lost in Debye waves R_d , the compression impulse R_c , and the impulse of expansion R_e of the closed shells. Since these are perfectly elastic, $R_c = R_e$, so that R is now given by

$$R = R_d + R_c + R_e = R_0(1 + \delta). \quad (3.7)$$

Since (3.3) is also valid in this collision case, the equation

$$V_1 - v_1 = -\delta(V_0 - v_0) \quad (3.8)$$

is obtained from (3.3), (3.4), and (3.7), which together with Eq. (3.1) is sufficient to determine the velocities v_1 and V_1 of the collision spheres after the collision. The result for the head-on collisions considered above is

$$\begin{aligned} v_1 &= \frac{m - \delta M}{m + M} v_0 + \frac{M(1 + \delta)}{m + M} V_0, \\ V_1 &= \frac{m(1 + \delta)}{m + M} v_0 + \frac{M - \delta m}{m + M} V_0. \end{aligned} \quad (3.9)$$

These equations are formally the same as the well-known equations for collisions with restitution, with the coefficient of restitution e replaced by the dissipation coefficient δ .

Since δ is connected with the excitation of Debye waves, it may be that δ is different for different ions and target atoms and for different crystallographic structures. It may also be that δ is somewhat different for sputtering with normal or with oblique ion incidence to the surface. This will be discussed later.

Equation (3.9) considers only head-on collisions for particles m and M which can move freely after the collision. If an upper surface atom is hit by the ion with a momentum component in the normal outward direction of the crystal, then this surface atom can move freely and thus can be ejected from the surface, provided the impulse is high enough to overcome the binding forces. Thus, for sputtering with oblique ion incidence, no other assumptions are necessary to derive the formulas for the threshold energies.

However, if the ion hits a lower surface atom the impulse is always directed inward to the bulk of the crystal. Thus a struck lower surface atom will immediately hit neighbors in the lattice lying in that direction, especially if the direction of the impulse is near to a close-packed direction. The struck atom is thereby stopped in its further movement into the lattice. The ion follows the path of the struck atom according to Eq. (3.9), if $m - \delta M > 0$, and will immediately collide again with the struck atom. But the closed shell of this atom is now in close contact with the closed shells

of its neighbors so that the target atom together with these neighbors acts like a solid wall. The result is that the ion rebounds even if the masses m and M do not obey the condition $m - \delta M < 0$.

The interference of the lattice neighbors in the collisions of the ion with lower surface atoms is taken into account by the additional assumption that for these collisions the mass of the struck lower atom is much greater than the mass M of the target element. With the introduction of this assumption, $m \ll M$, the threshold energies for sputtering at normal ion incidence on the crystal surface can easily be derived.

4. CATHODE SPUTTERING AT OBLIQUE ION INCIDENCE

Wehner² demonstrated the effect of obliquely incident ions, first discovered by Fetz,¹⁰ by sputtering a thin metal strip in a plasma of high density and low gas pressure and by catching the deposits on a glass cylinder surrounding the strip symmetrically. He proved, by covering one side of the specimen along one edge with Aquadag, that the four spots on the glass cylinder were produced by a small seam along the edges of the thin target strip. Here the ion sheath surrounding the target follows the contours around the edges of the specimen and causes oblique incidence of the ions on the target, while the ions in the center part of the ion sheath hit the target surface in the perpendicular direction. The upper left spot disappeared after the right upper edge was covered with Aquadag. The ejections of the surface atoms by obliquely incident ions occur in directions oblique to the surface [Fig. 1(a)] but on the other side of the normal to the incidence plane and at a considerably lower ion energy than the threshold energy of the target for normal ion incidence. It is further remarkable that the angular areas of the spots become larger with increasing ion energy.

4.1. Single Collision Sputtering at Oblique Ion Incidence

These interesting phenomena connected with oblique ion incidence can easily be explained in all details by applying the concepts developed above to a single collision between the impinging ion and an upper surface atom.

The plane of the drawing in Fig. 2 is the plane of incidence of the ion m impinging in an oblique direction on the $\{110\}$ plane of a face-centered cubic single crystal. The upper surface atoms M_1 , M_2 , and M_3 lie along the $\langle 100 \rangle$ direction, so that the separation s between these atoms is equal to the lattice constant a . Two atoms are indicated in the first lower plane, one of these being labeled M_L ; in the second lower plane three atoms are also shown in the drawing. The collision radius c_M of the target atoms and the separations s from each other are chosen proportional to an assumed

¹⁰ H. Fetz, Z. Physik 119, 590 (1942).

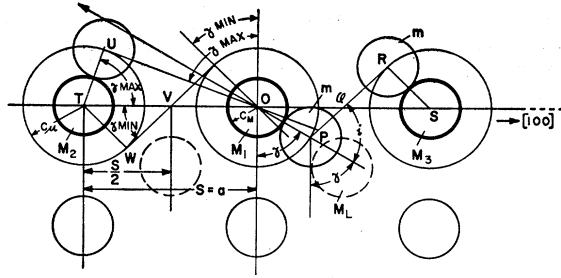


FIG. 2. Oblique ion incidence on an fcc $\{110\}$ surface. The surface row of atoms lies in the $\langle 100 \rangle$ direction. The upper surface atom M_1 is sputtered in a direct oblique collision if the ion m hits M_1 at certain contact points of its inside hemisphere with sufficient energy to overcome the binding forces of M_1 to the lattice.

value of the collision radius for Cu of $c_M = 0.68$ Å, as justified in Sec. 8, and the lattice constant $a = 3.608$ Å for Cu. The collision radius c_m of the ion m is assumed to be the same as c_M .

With these assumed values it can be seen from Fig. 2 that the collision sphere of the ion m , when impinging in the direction RP as drawn, can hit the collision sphere of the upper surface atom M_1 with the angle of incidence i directly on its inside half without being disturbed by the atom M_3 or by the lower atoms M_L , which do not lie in the plane of the drawing. Other contact points between the two collision spheres and other angles of incidence are possible and will be discussed later.

The collision in Fig. 2 is treated as an oblique collision between two perfectly elastic smooth spheres m and M with energy loss during the collision in the form of Debye waves as explained above, when introducing the dissipation coefficient δ . The sphere m has the initial velocity v_0 and M is assumed to be at rest before collision, thus $V_0 = 0$.

If i is the angle of incidence, i.e., the angle between the direction of m before the collision and the center line between m and M at the moment of contact, then M is moving in the direction of this center line after the collision, because the tangential components of the velocities and m and M are not changed in the collision; thus $v_{1t} = v_{0t}$ and $V_{1t} = V_{0t} = 0$. Therefore momentum is transferred only in the direction of the normal component of v_0 , which is $v_{0n} = v_0 \cos i$ and has the direction of the center line. Thus the velocity V_1 of the target atom M is given from Eq. (3.9) by

$$V_1 = \frac{m(1+\delta)}{m+M} v_0 \cos i. \quad (4.1)$$

4.2. Threshold Energy Formula for Single-Collision Sputtering

If γ is the angle of this center line with the normal to the surface, then the momentum component of M_1 in the normal direction outward to the surface is

$P = MV_1 \cos \gamma$, from which the energy transferred in this direction is $P^2/2M$. If this energy is equal to or greater than the heat of vaporization ΔH_{hkl} with which the atom M_1 in the crystal plane (hkl) is bound to the lattice, and which acts perpendicularly inward, then the atom M_1 will be sputtered. The heat of vaporization ΔH_{hkl} is different in different planes (hkl) and can be estimated from the available values ΔH_{298} for the different planes from the number of nearest neighbors given by the system, as will be shown below under 5.4.2.

The minimum ion energy $E_{\min} = \frac{1}{2}mv_0^2$ necessary to produce sputtering and defined as the threshold energy, is the energy for which the equation $\frac{1}{2}MV_1^2 \cos^2 \gamma = \Delta H_{hkl}$ holds with the value of V_1 from Eq. (4.1). The threshold energy at oblique ion incidence is therefore given by the equation

$$E_{\min} = \frac{(m+M)^2}{mM} \times \Delta H_{hkl} \times \frac{1}{(1+\delta)^2 \cos^2 \gamma \cos^2 i}. \quad (4.2)$$

Only a single collision of the impinging ion with an upper surface atom is involved in this formula. The angle γ determines the contact point of the ion on the lower half of the atom M_1 , and may be called "contact angle" for brevity. Different contact angles can lead to sputtering. For each of these angles γ , the threshold energy E_{\min} depends also on the incidence angle i , the lowest value of E_{\min} occurring for the smallest angle i , as seen from Eq. (4.2). The minimum value of the angle i is determined by the position of the atom to be sputtered in relation to the lattice neighbors in the incidence direction of the ion. Assuming, for instance, that the surface of the grain at which oblique ion incidence occurs is a $\langle 110 \rangle$ crystal plane, then the incident plane of the ion, which is perpendicular to the surface, can cut the $\langle 110 \rangle$ area of an elementary cube in different directions according to the orientation of the grain. Considering the main directions in the elementary area only, the rows of upper surface atoms have the separation $s = \frac{1}{2}a\sqrt{2}$ for the $\langle 110 \rangle$, $s = a$ for the $\langle 100 \rangle$, $s = \frac{1}{2}a\sqrt{6}$ for the $\langle 211 \rangle$, and $s = a\sqrt{3}$ for the $\langle 111 \rangle$ direction. In Fig. 2 the $\{110\}$ plane of a face-centered cubic crystal is drawn with the incidence plane of the ion m in the $\langle 110 \rangle$ direction, the separation of the upper surface atoms M_1 , M_2 , and M_3 thus being $s = a$. The drawing is also representative for multiples of a for s , which show up when atoms of this upper row have been sputtered. For the smallest separation $s = \frac{1}{2}a\sqrt{2}$, occurring in the $\langle 110 \rangle$ direction of the $\{110\}$ surface, the situation is different. The ion m cannot come in contact with the lower half of the collision sphere c_M at any angle of incidence, because in this case $s < 2c_M$.

As seen immediately from Fig. 2, the smallest angle of incidence i for each contact angle on the collision sphere c_M is the one at which the ion m can just freely pass the neighbor (atom M_3) on the incidence side.

4.3. Plots of the Minimum Threshold Energies for Different Contact Angles and Surface Atom Separations

In order to calculate the lowest possible threshold energies for each angle γ , the smallest angle i , as drawn in Fig. 2, must be taken for each s . In this case the relation

$$\cos(\gamma+i) = -(c_\mu/s)(1+\sin i) \quad (4.3)$$

can easily be derived from the triangles OPQ and QRS in Fig. 2, where $c_\mu = c_m + c_M$. With the aid of Eqs. (4.2) and (4.3) the minimum threshold energies can be calculated and plotted as a function of γ for different s , if the value for the coefficient of dissipation δ and the heat of vaporization ΔH_{110} in the $\{110\}$ plane for Cu are known. It is shown under 5.4.2 that the heat of vaporization can be assumed to be $\Delta H_{110} = 0.635\Delta H_{298}$, and from the later-calculated threshold energies for perpendicular ion incidence it can be seen that a value of $\delta = 0.54$ would be in agreement with experimental data on the threshold energy of Cu for normal ion incidence.

Since the angle between the ejection direction of the sputtered atom and the surface normal is the same as the contact angle γ , it is also possible to determine the maximum and minimum direction angles in which surface atoms can be expected to be ejected at oblique ion incidence. These limiting angles γ_{\max} and γ_{\min} can be read from the triangles TOU and TVW in Fig. 2, and are determined by $\cos \gamma_{\max} = c_\mu/s$ (4.4) and $\sin \gamma_{\min} = (2Tc_\mu/s)$ (4.5). Since γ_{\min} is determined by the tangent between the c_μ spheres of M_3 and M_1 , or as drawn between M_1 and M_2 , this minimum cannot really be reached, because of $\cos i = 0$, thus making E_{\min} from Eq. (4.2) infinite. At γ_{\max} the sputtered atoms can freely pass the nearest neighbor M_2 on the ejection side.

In Fig. 3 some curves of the threshold energies E_{\min} , calculated with the data for Cu as mentioned above, are plotted *versus* the contact angle γ for different separations s of various atom rows in a $\{110\}$ face-centered cubic plane. The minimum threshold energies are considerable lower for the larger separations than for the smaller ones. The influence of the sum of the collision radii c_μ of the ion and the target atom is also shown in the two curves for $s=a$. This factor is important only for smaller s . The curve with the largest value of $s=50a$ is drawn to demonstrate that the decrease of the lowest values of E_{\min} for a still larger s is very small.

The results are similar for other crystal planes and surface atom rows in other directions.

4.4. Comparison of the Results with Experimental Data

The surprising observation of Wehner¹ that at oblique ion incidence the atoms of the target are ejected in a direction away from the direction of the incident ions

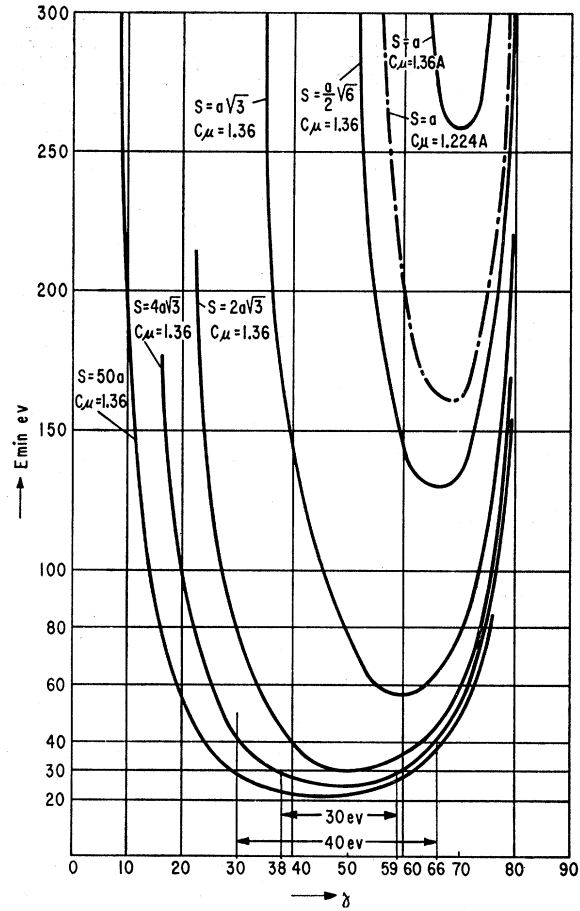


FIG. 3. Threshold energies at oblique ion incidence, plotted as a function of the ejection angles γ against the surface normal of a $\{110\}$ fcc plane for different separations s of upper surface atoms in the incidence plane of the ion. c_μ is the sum of the collision radii c_m and c_M of the ion m and the target atom M , respectively.

is self-explanatory from the assumed mechanism that the surface atom to be ejected must be hit on its inside half by the ion. Since the impulse transferred from the ion to the upper surface atom in the collision has the direction of the center line of the two particles at the moment of contact, the direction of the sputtered atom must be away from the incidence direction of the ion.

The explanation for the threshold energy being considerably lower than for sputtering at normal incidence, is given by the curves in Fig. 3, which are calculated for a $\{110\}$ plane of Cu. As soon as sputtering has started and atoms have been ejected, the separation of the atoms in the rows becomes greater—for instance, $2a$, $3a$, or even larger in the $\langle 100 \rangle$ direction or $2a\sqrt{3}$ and $4a\sqrt{3}$ in the $\langle 111 \rangle$ direction of the $\{110\}$ plane. As seen from the curves for these values in Fig. 3, the threshold energy for Cu at certain angles can be as low as 25 to 30 eV. This is considerably lower than the threshold energy for Cu at normal ion incidence, which is between 50 and 70 eV, as measured by Wehner.²

A third important experimental fact, reported by

Wehner,¹ concerns the increase of the angular area of the deposits towards the normal direction to the surface (smaller contact angle γ), when increasing the ion energy and keeping the ion sheath thickness constant. In this case the two separate spots on the glass cylinder, originating from one side of the target sheet, are brought closer and closer together. This fact can immediately be derived from the curves in Fig. 3. For a certain ion energy, for instance 100 ev, the contact angles γ belonging to the part of the curve below the 100-ev ordinate, are favorable for sputtering. If a certain mean value of s is assumed, then the angular area of γ in the curve belonging to s is seen to increase from a small area at the minimum threshold energy to the largest area at the assumed 100-ev ordinate. This means, since γ is measured from the surface normal to the spot, that the deposits lying symmetrically to the normal are brought closer and closer together. This explains satisfactorily the observations of Wehner.¹

However, as seen from the curves, there is also a smaller increase of the angular area of γ towards larger angles up to the limiting angle $\gamma_{\max}=80$ degrees, approximately. On the other hand, the curve drawn for the very large separation $s=50a$, shows that an angular area close to the surface normal of about ± 10 degrees cannot be reached by sputtered atoms, even at ion energies of 300 ev, if only oblique ion incidence is considered.

The real reason that the deposits merge together at higher ion energy to form only one extended spot on each side of the metal strip, as observed by Wehner,¹ is the fact that, at 50 to 70 ev for Cu, sputtering already occurs from ions hitting the center parts of the metal strip in the normal direction of incidence and ejecting atoms in the direction normal to the surface. This may be responsible for filling up the region around the surface normal on the glass cylinder.

The angular areas of the contact angle γ , for the ion energies 30 ev and 40 ev, taken from the second largest curve in Fig. 3, are drawn in Fig. 4 on the glass cylinder on which deposits are collected from a metal strip

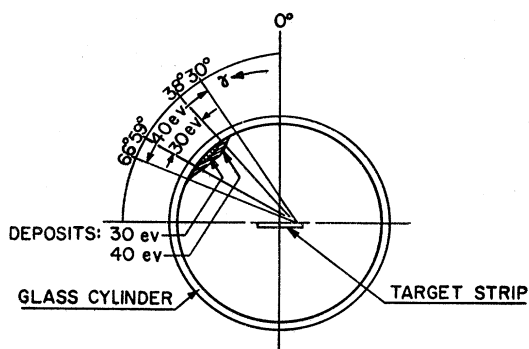


FIG. 4. Locations of the deposits on the cylindrical collector around the target in experiments with 30 and 40 ev as taken from the curves of Fig. 3.

placed symmetrically in the center of the cylinder. A comparison of Fig. 4 with the photographs of the spots in Wehner's paper,¹ in which the length of the photographs is very close to half the inner circumference of the cylinder, reveals that the calculated area of the deposits is in excellent agreement with the experimental data.

5. CATHODE SPUTTERING AT PERPENDICULAR ION INCIDENCE

Exclusively perpendicular ion incidence can be assumed if the target is a cylinder with a sufficiently large diameter. Wehner² used such cylindrical targets in the measurements of the threshold energies of 26 metals with Hg-ions at normal ion incidence.

To explain the sputtering phenomena at perpendicular ion incidence, it must be assumed that collisions leading to sputtering are multiple collisions of the ion with surface atoms, in which the direction of the ion is reversed so that in the final collision an upper surface atom can be hit on its inside half. The simplest assumption is that the ion collides first with a lower surface atom which, when hit at a certain contact point of its collision sphere, causes the ion to rebound in such a direction that an upper surface atom is hit on its inside half in this second collision. A certain energy loss in the form of excited Debye waves is involved in the first collision as explained in Sec. 3. An atom will be ejected in the second collision only if the remaining energy of the ion is large enough to transfer a momentum component to the upper atom in a normal outward direction with an energy equal to or greater than the binding energy of this atom to the crystal plane, which is assumed to equal the heat of vaporization.

5.1. General Threshold Energy Formula for Normal Ion Incidence

The theory of sputtering collisions with energy dissipation as developed in Sec. 3 offers a simple way to arrive at a formula for the threshold energy, when applied, according to the concepts developed above, to the two consecutive collisions of the ion (mass m): the first collision with a lower target atom and after rebound the second one with an upper target atom (mass M). Both kinds of particles are considered as perfectly elastic spheres while the energy loss is determined by the coefficient of dissipation δ . In Fig. 5(a) a unit area of a face-centered cubic (110) plane is represented in a top view. Figure 5(b) shows the plane $A-A$ perpendicular to the (110) surface with the upper surface atoms M_U , M_{U1} and the lower one M_L . The radii of the collision spheres of the ion and the target atoms may be c_m and c_M , respectively; the angle α between the surface normal and the center line of the atoms M_U and M_L is equal to 60 degrees in this case. Two possible collisions of the ions m and m' as indicated in the drawing are produced by different angles of

incidence i_1 on the lower atom M_L . The ion m rebounds at the reflection angle r_1 and hits the atom M_U at a contact point on its collision sphere determined by the angle γ , which is the angle between the surface normal and the center line of the particles at the moment of contact. The angle of incidence in this second collision is i_2 . Since the angles of incidence for the ions are chosen arbitrarily, the collisions involved are in general oblique collisions; only the second collision of the ion m' is a head-on collision with $i_2=0$.

For an oblique collision between two smooth perfectly elastic spheres m and M with an assumed coefficient of dissipation δ and with the velocities v_0 and V_0 before the collision, the velocities v_1 and V_1 of the particles after the collision are determined by the condition of smoothness which requires the following equations for the tangential components of the velocities: $v_{1t}=v_{0t}$ and $V_{1t}=V_{0t}$. For the normal components v_{1n} and V_{1n} the equations for head-on collision (3.9) apply; thus,

$$v_{1n} = \frac{m - \delta M}{m + M} v_{0n} + \frac{M(1 + \delta)}{m + M} V_{0n}, \quad (5.1)$$

$$V_{1n} = \frac{m(1 + \delta)}{m + M} v_{0n} + \frac{M - \delta m}{m + M} V_{0n}. \quad (5.2)$$

The target atom M is always assumed to be at rest before the collision; thus $V_{0n}=0$. Since the components of v_0 at the incidence angle i are $v_{0n}=v_0 \cos i$ and $v_{0t}=v_0 \sin i$, the velocity v_1 of the ion m after the collision is given by

$$v_1^2 = v_{1n}^2 + v_{1t}^2 = v_0^2 \left[1 - \frac{2mM(1 + \delta) + M^2(1 - \delta^2)}{(m + M)^2} \cos^2 i \right], \quad (5.3)$$

while the velocity V_1 , acquired by the atom M in this collision, is

$$V_1 = \frac{m(1 + \delta)}{m + M} v_0 \cos i. \quad (5.4)$$

With these formulas the problem of double collisions at normal ion incidence can be solved immediately. In the first collision of the ion m , the lower surface atom M_L in Fig. 5(b) is hit at the incidence angle i_1 ; the ion then rebounds at the angle of reflection r_1 against the atom M_U which is hit in an oblique collision with the incidence angle i_2 . Since the lower surface atom M_L is not freely movable as explained under 3, the condition $m \ll M$ must be applied to Eq. (5.3) for this collision. This leads to the equation for the velocity v_1 of m after the collision:

$$v_1^2 = v_0^2 [1 - (1 - \delta^2) \cos^2 i_1]. \quad (5.5)$$

In the second collision the velocity V_2 of the atom M_U after the collision is of interest. Substituting v_1 , V_2 , and i_2 for v_0 , V_1 , and i , respectively, in Eq. (5.4), V_2

becomes

$$V_2 = \frac{m(1 + \delta)}{m + M} v_1 \cos i_2. \quad (5.6)$$

Since the angle between the surface normal and the center line of m and M_U at the moment of contact is γ , the normal component of the momentum transferred to M_U in this collision is $P = MV_2 \cos \gamma$; thus the energy acquired by M_U is correspondingly $(P^2/2M) = \frac{1}{2}(MV_2^2) \cos^2 \gamma$. The atom M_U is subject to binding forces, determined by the attractive forces of its neighbors in the lattice, acting in the normal inwards direction and generally assumed to be equal to the heat of vaporization ΔH_{hkl} in this lattice plane. Thus, only if the energy transferred to M_U in the collision is equal to or greater than ΔH_{hkl} , can the atom M_U be removed from the surface. If E_{\min} is the lowest primary energy at which this happens and is thus equal to $\frac{1}{2}mv_0^2$, this leads with the aid of Eqs. (5.5) and (5.6) to the following formula:

$$E_{\min} = \frac{(m + M)^2}{mM} \times \Delta H_{hkl} \times \frac{1}{(1 + \delta)^2 \cos^2 \gamma \cos^2 i_2 [1 - (1 - \delta^2) \cos^2 i_1]}. \quad (5.7)$$

This is the general equation for the threshold energy at normal ion incidence under the assumed double-collision mechanism.

5.2. Discussion of the General Threshold Energy Formula for Normal Ion Incidence

From Fig. 5(b) it can be immediately seen that the angles γ , i_1 , and i_2 occurring in formula (5.7) are dependent on the sizes of the collision radii c_m and c_M , the separation between the atoms M_U and M_L , and the angle α between the surface normal and the center line of M_U and M_L . The separation $M_U - M_L$ and the angle α are determined by the lattice constant a , the crystal system, and the plane under investigation. Because of the present lack of the required data for the coefficient

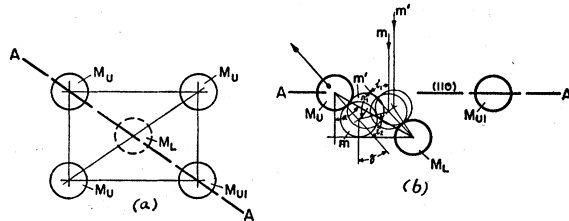


Fig. 5. (a) Top view of the unit area of a (110) fcc single-crystal plane. (b) Double collision sputtering in the plane $A-A$ perpendicular to the (110) fcc plane of Fig. 5(a). The ion m hits the lower atom M_L , rebounds against the upper atom M_U , and ejects M_U if the energy of m is high enough to overcome the binding forces of M_U to the lattice.

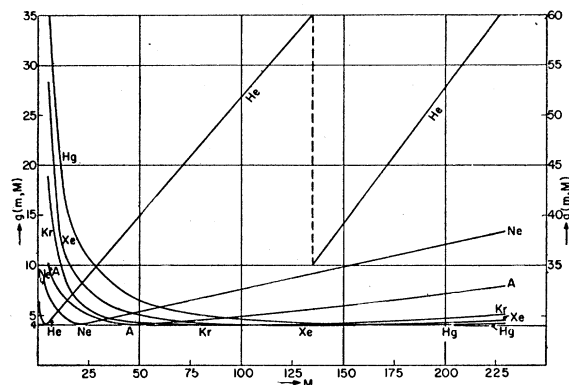


FIG. 6. Plot of the mass factor $g(m, M) = (m+M)^2 / mM$ vs atomic weight of the target atoms M for different ions m .

of dissipation and for the collision radii, a general solution has not been carried out.

In order to check the approximation, as developed in the next paragraph, some values have been calculated with the data applying to Al; the collision radii were taken equal to the ion size of Al for both the target atom and the impinging ion; the separation between the atom M_U and M_L was taken according to the fcc lattice with $a = 4.04$ Å, and the coefficient of dissipation was chosen with $\delta = 0.5$. The result was that the lowest threshold energy occurs between 35 and 42 degrees of the incidence angle i_2 , and the minimum threshold energy as calculated from Eq. (5.7) is only 12% lower than the threshold energy calculated from the simplified formula (5.11) under 5.3. Since the available data on threshold energies as seen from the table of Wehner² have considerably larger fluctuations, the simplified formula for the threshold energies as derived below is well able to lead to values in agreement with the experimental data.

5.3. Simplified Threshold Energy Formula at Normal Ion Incidence

To simplify the calculation, only one special collision is taken into account, namely the one for which

$$i_1 + r_1 = \alpha, \quad (5.8)$$

where α is the angle between the surface normal and the center line of the lower and the upper surface atom involved in the collision, as indicated in Fig. 5(b). This condition corresponds to the case in which the lower atom M_L is replaced by a plane at the center of the lower atom with an angle of inclination i_1 of its normal from the surface normal and the ion m impinges on this plane in a perpendicular direction to the surface. In this case the angles i_1 and r_1 are connected with each other by the equation

$$\tan i_1 = \delta \tan r_1, \quad (5.9)$$

so that i_1 can be calculated for each angle α and each

value of δ from the quadratic equation resulting from (5.8) and (5.9), with the solution

$$\tan i_1 = -\frac{1+\delta}{2 \tan \alpha} + \left[\frac{(1+\delta)^2}{4 \tan^2 \alpha} - \delta \right]^{1/2}, \quad (5.10)$$

since only the positive sign of the square root has physical significance.

Since in this case Eq. (5.6) holds with $i_2 = 0$ and $\gamma = \alpha$, the general threshold energy formula (5.7) is reduced for the special " α -collision" to

$$E_{\min} = \frac{(m+M)^2}{mM} \times \Delta H_{hkl} \times \frac{1}{(1+\delta)^2 \cos^2 \alpha [1 - (1-\delta^2) \cos^2 i_1]}, \quad (5.11)$$

where i_1 is determined by Eq. (5.10) for each α and δ . For any low-index crystal plane (hkl), the angle α can easily be calculated from the crystal system. The heat of vaporization ΔH_{hkl} in this plane can be determined for the target material from the value ΔH_{298} , as shown below. Thus, if a reasonable assumption is made for the coefficient of dissipation, for instance $\delta = 0.5$, the calculations of the threshold energies for different target metals and ions can be carried out with Eq. (5.11).

5.4. Discussion of the Simplified Threshold Energy Formula for Normal Ion Incidence

Equation (5.11) may be rewritten in the form

$$E_{\min} = g(m, M) \Delta H_{hkl} f(\alpha_{hkl}, \delta), \quad (5.12)$$

with the mass factor

$$g(m, M) = (m+M)^2 / mM \quad (5.13)$$

and the factor

$$f(\alpha_{hkl}, \delta) = \frac{1}{(1+\delta)^2 \cos^2 \alpha_{hkl} [1 - (1-\delta^2) \cos^2 i_1]}, \quad (5.14)$$

where the index (hkl) indicates that the angle α is different for different low-index crystal planes, and the only angle of incidence involved in (5.11) is now labelled i .

5.4.1. Mass Factor $g(m, M)$

This factor has been plotted in Fig. 6 as a function of the target mass M for different ions such as He, Ne, Ar, Kr, Xe, and Hg. If the coefficient of dissipation δ were the same for different combinations of ions with the same target element, then the threshold energy values for other ions would only depend on this mass factor $g(m, M)$, since the factors f and ΔH_{hkl} are then the same for each ion-target element combination. Thus, the threshold energies could be immediately predicted for other ions from the values for Hg ions with the aid of plots of $g(m, M)$ in Fig. 6. However, the permissibility of such a procedure is questionable at

the present time, since no measurements of threshold energies with ions other than Hg, with the same precautions, are known in the literature. On the other hand, much more refined measurements of the threshold energies are probably necessary to decide whether or not the coefficient of dissipation is the same for each ion-target combination.

5.4.2. Heat of Vaporization ΔH_{hkl}

Values of the heat of vaporization for special single crystal planes (hkl) are not known in the literature. The only known are the average values ΔH_{298} for polycrystalline materials at 298°K (Quill¹¹) giving the heat in kilocalories to vaporize one mole of the material.

In a low-index single crystal plane (hkl) the binding energy ϕ_{hkl} of an upper atom to the bulk can be assumed in a first approximation to be proportional to the number of nearest neighbors. To obtain a rough estimation of ΔH_{hkl} from ΔH_{298} , the unit area of a polycrystalline surface is assumed to be composed exclusively of equal areas of the {100}, {110}, and {111} crystal planes. The total surface energy of a unit area of this surface would then be given by the average $(N_{hkl}\phi_{hkl})_{Av} = \frac{1}{3}(N_{100}\phi_{100} + N_{110}\phi_{110} + N_{111}\phi_{111})$, where N_{100} , N_{110} , and N_{111} are the numbers of upper surface atoms per unit area in the corresponding low-index planes.

The ratio $\Delta H_{hkl}:\Delta H_{298}$ is then equal to the ratio of the product $N_{hkl}\phi_{hkl}$ to the average $(N_{hkl}\phi_{hkl})_{Av}$.

This leads to the equation

$$\Delta H_{hkl} = \Delta H_{298} \times \frac{N_{hkl}\phi_{hkl}}{(N_{hkl}\phi_{hkl})_{Av}}, \quad (5.15)$$

which can be easily evaluated for the low-index planes in different crystal systems. Considering only the nearest neighbors, for instance, the resulting values are as follows:

for bcc systems:	for fcc systems:
$\Delta H_{100} = 0.81\Delta H_{298}$,	$\Delta H_{100} = 1.03\Delta H_{298}$,
$\Delta H_{110} = 1.72\Delta H_{298}$,	$\Delta H_{110} = 0.635\Delta H_{298}$,
$\Delta H_{111} = 0.47\Delta H_{298}$,	$\Delta H_{111} = 1.335\Delta H_{298}$.

If nearest and second nearest neighbors are considered, the numbers would be 0.93, 1.47, and 0.60, respectively, for bcc systems and 1.13, 0.67, and 1.20, respectively, for fcc systems. The assumption that the energy values are proportional to the number of nearest neighbors can be considered as a permissible approximation for the metallic bond and is used in the calculations. As could be expected, the values are higher in the most densely populated planes such as {110} in bcc systems and {111} in fcc systems.

¹¹ L. L. Quill, *The Chemistry and Metallurgy of Miscellaneous Materials; Thermodynamics* (McGraw-Hill Book Company, Inc., New York, 1950), first edition, p. 26.

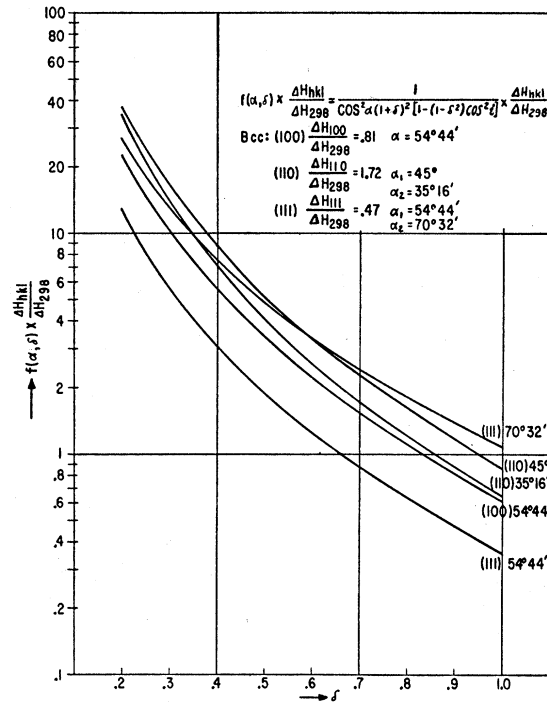


FIG. 7. Plot of the function $f(\alpha, \delta) \times \Delta H_{hkl} / \Delta H_{298}$ for the lattice angles α occurring in unit areas of low indices planes of bcc crystals.

5.4.3. Factor $f(\alpha_{hkl}, \delta)$

This factor, defined by Eq. (5.14), can be calculated for the different angles α_{hkl} occurring in the low-index planes of different crystal systems. The results are plotted in Fig. 7 and Fig. 8 for bcc and fcc systems, respectively, multiplied for convenience by the factor $\Delta H_{hkl} / \Delta H_{298}$. Since the threshold energy in formula (5.12) can be rewritten in the form

$$E_{min} = g(m, M) \times \Delta H_{298} [\vartheta(\alpha_{hkl}, \delta) \Delta H_{hkl} / \Delta H_{298}], \quad (5.17)$$

it can be readily calculated for each plane (hkl). The value of $g(m, M)$ can be taken from Fig. 6 for the ion-target combination, the bracket value from Fig. 7 or Fig. 8, and the heat of vaporization ΔH_{298} from the tables and may be converted into ev. In this case the threshold energy is obtained in ev, since the other two factors are dimensionless.

5.5. Threshold Energies for Polycrystalline Target Materials at Normal Ion Incidence

In the calculations of threshold energies for polycrystalline target materials without preferred orientations of the surface grains, an average value of the function $f(\alpha_{hkl}, \delta) \Delta H_{hkl} / \Delta H_{298}$, taken over all the angles occurring in the crystal system of the target, may be chosen from Fig. 7 or Fig. 8 for the assumed value of the coefficient of dissipation δ . If, however, preferred orientations are present, for instance as in cold-rolled fcc metal sheets where (110) orientation is prevailing,

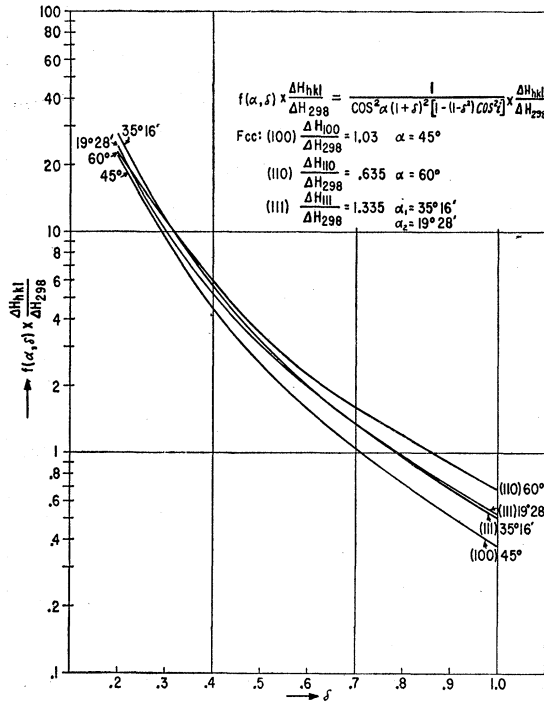


FIG. 8. Plot of the function $f(\alpha, \delta) \times \Delta H_{hkl} / \Delta H_{298}$ for the lattice angles α occurring in unit areas of low indices of fcc crystals.

then the value from Fig. 8 should be taken closer to the angle α belonging to the (110) plane for which $\alpha = 60^\circ$.

5.6. Agreement of the Simplified Threshold Energy Formula with Experimental Data

Wehner² determined experimentally the threshold energies for 26 different polycrystalline metals in Hg gas discharge, using targets in the form of cylinders with a sufficiently large diameter to assure normal ion incidence exclusively, and observing all the precautions necessary to avoid back diffusion of the sputtered atoms to the surface. If the threshold energy formula (5.12) is applied to the seven bcc and ten fcc metals of his table, and the values of $g(m, M)$ and average values of $f(\alpha_{hkl}, \delta) \Delta H_{hkl} / \Delta H_{298}$ are taken from Figs. 6, 7, and 8, respectively, for an assumed coefficient of dissipation $\delta = 0.5$, then the resulting threshold energies for all these metals are well in the ranges of the experimental data.

This can be seen from Table I, in which the values of the function $f(\alpha_{hkl}, \delta) \Delta H_{hkl} / \Delta H_{298}$ are calculated for the lower and upper limits of the threshold energies determined by Wehner,² and the corresponding values for the coefficient of dissipation δ are read from Figs. 7 and 8, respectively. The values for bcc metals are found to be between $\delta = 0.5$ and $\delta = 0.63$, while the values for fcc metals are between $\delta = 0.39$ and $\delta = 0.54$, indicating a higher energy loss by excitation of Debye waves in fcc lattices compared with that in bcc lattices.

The widespread limits of the threshold energies in Wehner's table² for some metals are due to the method of evaluating the threshold energies from the sputtering rate data. Refined methods of measuring the threshold energies are probably necessary to determine to what degree the coefficient of dissipation is different for different targets sputtered with the same kind of ions, or *vice versa*, for the same target atoms sputtered with different ions.

6. THRESHOLD ENERGY FORMULA FOR TRIPLE-COLLISION SPUTTERING AT NORMAL ION INCIDENCE

In studies of the spot patterns¹² of {110} fcc crystal planes, it can be observed that already at relatively low ion energies some of the upper surface atoms are ejected in a direction normal to the crystal plane. These produce a center spot in the spot patterns. An upper atom, sputtered in the normal outward direction, must have been hit by an ion at its lowest inside point with a sufficiently large momentum component in the normal outward direction. The fact that this center spot, at somewhat higher ion energy than the threshold, is more pronounced than the spots belonging to the α directions in the unit areas, indicates that a special mechanism is effective after some surface atoms have been removed from the surface by the sputtering process.

This mechanism may be described with the aid of Fig. 9(a) and Fig. 9(b). The first drawing is a top view of a {110} fcc single-crystal plane orientated in the plane of the drawing so that one of the (111) directions is vertical. The unit areas are rectangles, as seen in this top view; sputtering occurs at low ion energy in the directions of the diagonals of the unit areas, when

TABLE I. Coefficients of dissipation, calculated from threshold-energy data on bcc and fcc metals sputtered with Hg-ions.

System	Element	$g(m, M)$	ΔH_{298} ev	E_{min} (Wehner ^a) ev	$f(\alpha, \delta)$ $\times \frac{\Delta H_{hkl}}{\Delta H_{298}}$	Coefficient of dissipation δ
bcc	V	6.18	5.2	120-130	3.75-4.06	0.52 -0.50
	Cr	6.11	3.68	60-80	2.68-3.56	0.57 -0.53
	Fe	5.84	4.2	60-70	2.44-2.84	0.63 -0.57
	Cb	4.70	7.6	120-130	3.39-3.68	0.55 -0.53
	Mo	4.56	6.75	80-100	2.6-3.26	0.59 -0.54
	Ta	4.08	8.7	120-140	3.44-4.1	0.54 -0.50
	W	4.01	8.75	80-100	2.88-2.86	0.625-0.57
fcc	Al	9.54	3.29	120-140	3.8-4.45	0.45 -0.425
	Ni	5.68	4.41	70-90	2.8-3.6	0.52 -0.48
	Cu	5.46	3.56	50-70	2.5-3.5	0.53 -0.47
	Rh	4.40	6.0	70-80	2.65-3.02	0.54 -0.50
	Pd	4.29	4.05	50-80	2.87-4.6	0.51 -0.42
	Ag	4.27	3.04	40-50	3.1-3.86	0.49 -0.46
	Pt	4.00	5.86	70-90	3.0-3.85	0.50 -0.45
	Au	4.00	3.94	40-50	2.55-3.18	0.53 -0.49
	Pb	4.00	2.02	20-40	2.48-4.95	0.54 -0.40
	Th	4.02	6.5	120-140	4.6-4.35	0.42 -0.39

^a See reference 2.

¹² E. B. Henschke, J. Appl. Phys. (to be published).

one of the lower surface atoms M_L is hit by the perpendicularly incident ion and rebounds against an upper surface atom M_U , ejecting it from the surface in this collision. If it is now assumed that the upper atoms M_{U1} , and M_{U2} have been sputtered by ions in collisions with the lower atoms M_{L1} , and M_{L2} , respectively, then a small furrow will have been generated in the surface in the direction $\langle 211 \rangle$. It is now possible and equally probably that an ion will hit a lower atom within this furrow, for instance one of the atoms lying perpendicularly under the atoms M_{U1} , and M_{U2} in the second lower plane, and rebound against the atom M_{L2} to eject it from the target. The angular conditions are the same as in the unit area of the $\{110\}$ surface, and the energy required is only a little higher since, after M_{U1} and M_{U2} have been sputtered, M_{L2} has only nine nearest neighbors and even only eight after M_{U4} has also been ejected, while an upper atom in the unit area of a $\{110\}$ plane has seven nearest neighbors.

In Fig. 9(b) the perpendicular plane $A-A$ in the $\langle 211 \rangle$ direction of Fig. 9(a) is drawn. After the lower surface atom M_{L2} of this plane has been removed as described, the intersection of the assumed electron cloud of the surface atoms with the paper plane, indicated by the curve c_0 for the undisturbed surface, is represented by the curve c_1 . If by the same mechanism the atoms M_{U4} , M_{L3} , M_7 , and M_8 are also sputtered, then the curve c_2 indicates the intersection of the electron cloud with the $\{111\}$ plane of the drawing; the cloud now follows the more extended side walls of the furrow, which are built up of staggered $\{110\}$ unit areas, the planes of which intersect the surface plane at an angle of 60° , and their diagonals M_6-M_{11} and $M_{11}-M_{10}$ lie in the plane of the drawing.

With the generation of these furrows in the surface, which have been observed in a more developed state in electron micrographs of sputtered $\{110\}$ single crystal planes of Ag at very low ion energy, a triple-collision mechanism is involved which leads to the ejection of upper atoms in the perpendicular direction to the surface, if the ion energy is only a small amount higher than the threshold energy for double-collision sputtering. This is easily explainable, as follows, with the aid of Fig. 9(b).

In the case of the smallest furrow (curve c_1), an ion m may hit the atom M_{U4} in the indicated direction, so that it rebounds against the atom M_5 and again rebounds against the upper surface atom M_{U3} , ejecting this atom in the direction of the arrow. If the curve c_2 can be assumed to apply, then a second ion m' may hit M_{10} and rebound against M_9 and again against M_6 in the normal outward direction. The directions in which the atoms M_5 and M_9 are hit by the ions m and m' , respectively, are perpendicular to the $\{110\}$ unit areas, which lie in the left side wall of the furrow; these two atoms are lower surface atoms in these unit areas.

Thus formula (5.11) for a double collision at normal ion incidence can be applied to the second and third

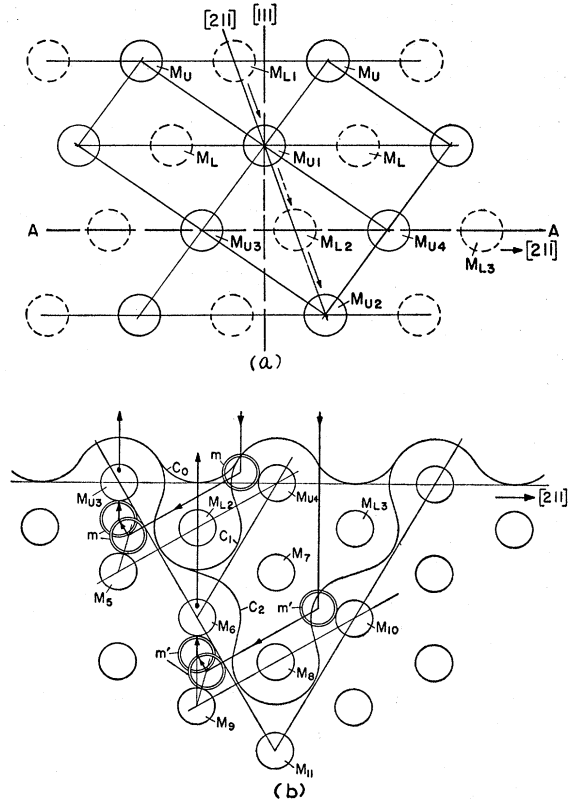


FIG. 9. (a) Triple-collision sputtering: furrow generation in an fcc $\{110\}$ single-crystal plane by consecutive sputtering of the upper atoms M_{U1} , M_{U2} , and the lower surface atom M_{L2} . (b) Triple-collision sputtering mechanism in the $\{111\}$ plane $A-A$ perpendicular to Fig. 9(a). The ions m and m' eject the atoms M_{U3} and M_6 , respectively, in the direction normal to the surface after two preceding collisions with surface atoms of the furrow.

collisions of the ions m and m' , impinging on a (110) plane. If the first collision of m with M_{U4} , and of m' with M_{10} is treated as a collision with an inclined plane (incidence angle i_1), then the velocity v_1 of the ion after this first collision is given by Eq. (5.5). In the application of formula (5.11) to the second collision, v_0 and v_1 must now be replaced by v_1 and v_2 and the angle i_1 by i_2 with v_1 from Eq. (5.5). This gives the equation for the threshold energy for the triple collision sputtering:

$$E_{\min} = \frac{(m+M)^2}{mM} \times \Delta H_{hkl} \times \frac{1}{(1+\delta)^2 \cos^2 \alpha [1 - (1-\delta^2) \cos^2 i_2] [1 - (1-\delta^2) \cos^2 i_1]} \quad (6.1)$$

Here α and ΔH_{hkl} have the same values ($\alpha=60^\circ$ and $\Delta H_{110}=0.635\Delta H_{298}$) for the m' triple collision as used in the double collision with the $\{110\}$ plane, while the value of ΔH_{hkl} for the triple collision of m is lower for the following reason. The upper atom M_{U3} , involved

in this collision, has lost the two nearest neighbors M_{U1} and M_{L2} (see Fig. 9a), so that ΔH_{hkl} for this atom, which lies on the edge of the furrow, is lower in the ratio of 5:7.

The angle of incidence i_1 for the first collisions of m and m' is determined by Eq. (5.10) with the angle $\alpha=120^\circ$ between the atoms $M_{U4}\rightarrow M_5$ and $M_{10}\rightarrow M_9$ and the surface normal. This gives the incidence angle $i_1=51^\circ 36'$ for an assumed value of $\delta=0.5$. With these values of i_1 and δ , the threshold energy for the triple collision calculated with Eq. (6.1) turns out to be only 40% higher than the threshold energy for the double collision in the $\{110\}$ plane, if the path of the ion m' in Fig. 9(b) is considered. Since the threshold energy, required for the triple collision in the m case, is five-sevenths of this amount, it is exactly the same as the threshold energy for the double collision in the $\{110\}$ plane.

The average threshold energy necessary for triple collisions may therefore be estimated to be approximately 25% higher than for double-collision sputtering of an undisturbed $\{110\}$ fcc plane; this is in good agreement with experimental results.

6.1. Triple Collisions in Sputtering Phenomena

Besides explaining the appearance of the center spot in the spot patterns of $\{110\}$ fcc single crystal planes,^{3,12} the triple-collision mechanism also explains some other phenomena observed in sputtering experiments. In sputtering carefully prepared single-crystal planes at low ion energy, holes often appear in the otherwise unattacked plane, which widen out rapidly and have extremely sharp contours, as seen in electron micrographs. The primary reasons that these crater-like holes appear at all are lattice defects where the threshold energy can be assumed to be lower. However, the enlargement of the craters and the very sharp contours can be explained by the triple mechanism as described with Fig. 9(b). The same is true for the preferential attack of grain boundaries in polycrystalline targets at low ion energy.

7. SPUTTERING RATE FOR CATHODE SPUTTERING AT LOW ION ENERGY

Besides the threshold energy the second important magnitude in cathode sputtering phenomena is the sputtering rate, defined as the number of sputtered atoms per incident ion.

Reliable measurements of the sputtering rate at low ion energies, as known from literature, are obtained by the method of Kingdon and Langmuir,⁶ using the decrease of the electron emission of thoriated tungsten, and by the method of Wehner and Medicus,¹³ using the displacement of the Langmuir probe characteristics for measuring the sputtering rate of Pt and Xe at very low ion energies. The last method gave the result, that

the sputtering rate S of Pt with Xe ions in the energy range $50 < E < 200$ ev is roughly proportional to $(E-E_0)^2$, with $E_0=40$ ev, where E_0 is determined as the intersection of the linear part of the \sqrt{S} versus E curve with the E axis and considered as the threshold energy. Two measured values of the sputtering rate at 35 ev and 30 ev, lying on the lower nonlinear part of the curve, were disregarded.

7.1. Sputtering Rate and Threshold Energy

The knowledge of a law for the sputtering rate, derived from a general theory of sputtering, is very important, because the more refined measurements of the threshold energies are based on measurements of the yield at constant ion current density for different ion energies obtained in a certain time interval (e.g., 10 minutes for higher ion energies). Much greater time intervals are necessary (30 minutes) near the threshold energy where the sputtering rate is small. If the curve of the sputtering rate S versus ion energy E is plotted, the upper part of the curve is found to be linear and the sputtering rate is proportional to $(E-E_0)$ if an energy value E_0 is determined by the intersection of the extended linear part with the abscissa. If the lower nonlinear part of the same curve is replotted with the square root of S versus E , then the upper part of this second curve is again linear, and another value E_0' can be obtained by the intersection of the extended linear part, indicating that the sputtering rate S in this part of the curve is proportional to $(E-E_0')^2$. The energy values E_0 and E_0' are considered as the threshold energies. There is no reason, in the opinion of the author, to define the values E_0 and E_0' as two different threshold energy values, one, E_0 , for the higher energy level from the S vs E curve, which may be 90 ev, as for Pt-Hg, and another E_0' for lower ion energies from the \sqrt{S} vs E curve, which may be 45 ev, and finally to take a range between these values.⁴ Neither the S curve nor the \sqrt{S} curve can be expected to cut the abscissa. This is not because there is an indetermination, but because the definition of the threshold energy, as the lowest ion energy at which sputtering occurs, implies that the sputtering rate is definitely not zero at the threshold energy. It becomes zero only if the ion energy is below the threshold energy. At lower ion energies than the threshold, atoms cannot be ejected from the surface. Thus, the lowest ion energy, at which a yield can be measured in a reproducible manner, must be regarded as the threshold energy. Threshold energies determined by the intersection of the linear part of the curves with the E axis, for which $S=0$, are therefore a little too high. The spot pattern experiments with single-crystal planes³ prove that there is no indetermination near the threshold energy due to lattice defects.

The main reason for the discrepancies in determining the threshold energy is the lack of a theory from which the curve of sputtering rate vs ion energy can be derived

¹³ G. Wehner and G. Medicus, J. Appl. Phys. 25, 693 (1954).

for the ranges from the threshold energy to a few multiples of it, in order to extrapolate the threshold energies in the right manner.

7.2. Definition of the Sputtering Rate of Single-Crystal Planes

Since the sputtering rate is defined as the ratio of the number of sputtered atoms to the number of incident ions, it can also be determined by the ratio of the sizes of the "favorable areas" on the crystal surface, which must be hit by the perpendicularly incident ions to produce sputtering, to the total area of the target hit by the ions. If the target is an ideal low-index single-crystal (hkl) plane, it is only necessary to consider this ratio in the unit area of this plane, A_{hkl} , which is the smallest area between upper surface atoms M_U containing only one lower surface atom M_L in the $\{100\}$ and $\{110\}$ planes and two lower atoms in different layers in the $\{111\}$ planes and covering the whole surface by simple translations. The number of favorable areas within the unit area is given by the number p_α of the angles α , which are the angles between the surface normal and the center lines between the lower and the upper surface atoms of this area. For instance, it is $p_\alpha=4$ in bcc and fcc $\{100\}$ planes and in $\{110\}$ fcc planes, $p_{\alpha_1}=2$ and $p_{\alpha_2}=2$ in $\{110\}$ bcc planes, and $p_{\alpha_1}=3$ and $p_{\alpha_2}=3$ in $\{111\}$ bcc and fcc planes.

In Fig. 10 the two atoms M_U and M_L of a unit area, lying in the α direction, are represented by the spheres with the radius c_M . Three ions m_1 , m_2 , and m_3 , with the radius of their collision spheres c_m , impinge on the lower atom M_L in the direction perpendicular to the surface of the plane and rebound against the upper atom M_U , as indicated in Fig. 10.

The centers of all the ions, which can hit the atom M_U after rebounding from the lower atom M_L in favorable directions for the ejection of M_U , lie within a certain area $A_{\mu\alpha}$ on the sphere with radius $c_\mu = c_m + c_M$ concentric with M_L . The projection $P(A_{\mu\alpha})$ of this area onto the surface plane, as drawn in a perspective representation, is then the favorable area on the surface of the crystal belonging to the represented α direction within the unit area. The size of this area depends on the energy of the ions. At the threshold energy the very small area $\Delta A_{\mu\alpha}$ on the c_μ sphere must be hit by the ion m , to produce one of the few collisions requiring the least amount of energy for sputtering M_U . The projection of this area on the surface is $P(\Delta A_{\mu\alpha})$. Since there are p_α of such favorable collision areas within each unit A_{hkl} , possibly with different angles $\alpha_1, \alpha_2, \dots$ and different values of $P(A_{\mu\alpha_1}), P(A_{\mu\alpha_2}), \dots$, the definition of the sputtering rate within a unit area of a single-crystal plane (hkl), introduced above, can be described by the equation

$$S_{hkl} = \sum_{\alpha}^{a_1, a_2, \dots} p_\alpha P(A_{\mu\alpha}) / A_{hkl} \quad (7.1)$$

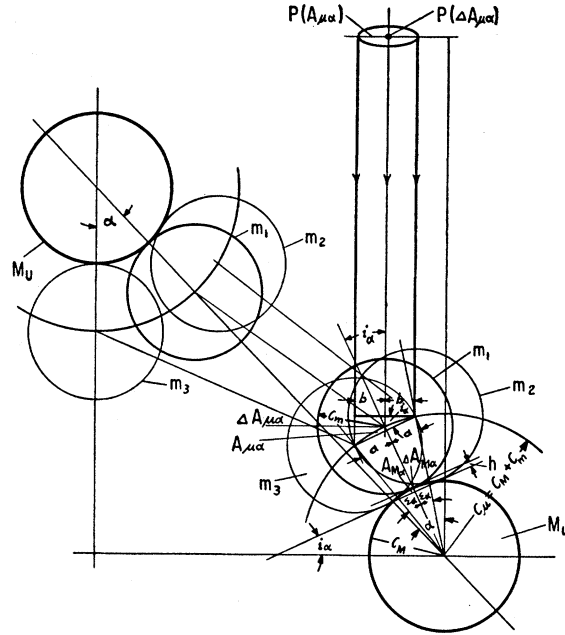


FIG. 10. Sputtering rate calculations for single-crystal planes. $P(A_{\mu\alpha})$ is one of the areas on the surface plane favorable for sputtering of the upper atoms M_U within a unit area A_{hkl} . $A_{M\alpha}$ is the corresponding area in the collision sphere of the lower surface atom M_L .

with the condition

$$(S_{hkl})_{\min} = \sum_{\alpha}^{a_1, a_2, \dots} p_\alpha P(\Delta A_{\mu\alpha}) / A_{hkl}. \quad (7.2)$$

A generalization of this definition for single crystal planes, in which the angles $\alpha_1, \alpha_2, \dots, \alpha_n$ and the numbers $p_{\alpha_1}, \dots, p_{\alpha_n}$ vary in different units areas or for surfaces of polycrystalline targets can easily be made and will be discussed later.

7.3. Sputtering Rate for Single-Crystal Planes (hkl) at Low Ion Energies

To find a relation between the sizes of the favorable areas $P(A_{\mu\alpha})$ and the ion energy E , two assumptions must be made, one about the shape of these areas and the other about the dependence of the size upon the ion energy E . If the area $A_{\mu\alpha}$ is assumed to be circular with radius a on the sphere with the radius $c_\mu = c_m + c_M$, then the projection of this area $P(A_{\mu\alpha})$ onto the surface plane, as seen from Fig. 10, is given by the equation

$$P(A_{\mu\alpha}) = \pi ab = \pi c_\mu^2 \sin^2 \epsilon_\alpha \cos(\pi - i_\alpha), \quad (7.3)$$

with

$$a = c_\mu \sin \epsilon_\alpha, \quad b = c_\mu \sin \epsilon_\alpha \cos(\pi - i_\alpha). \quad (7.4)$$

After the incidence angle i_α , which is always acute, has been defined as the angle between the normal to the surface and the center line of the colliding spheres at the moment of contact, the angle between the center line and the surface is $(\frac{1}{2}\pi - i_\alpha)$. Since the radius a ,

lying in the plane of the drawing, is perpendicular to this center line, the projection angle of this radius against the surface is $(\pi - i_\alpha)$.

The smallest areas $\Delta A_{\mu\alpha}$ of $A_{\mu\alpha}$ and thus $\Delta A_{M\alpha}$ of $A_{M\alpha}$ on the c_M collision sphere of the target atom M_L apply for the threshold energy E_{\min} . For simplification, it is assumed that the collision happens at the incidence angle i_α belonging to E_{\min} producing the collision as explained in the simplified double-collision theory above, where α is given by the lattice structure of the unit area. With increasing energy E , the very small area $\Delta A_{M\alpha}$ is enlarged to $A_{M\alpha}$ since the ions hitting the target atom in the neighborhood of $\Delta A_{M\alpha}$ are also able to produce sputtering at incidence angles deviating only within certain small limits from the small circular area $\Delta A_{M\alpha}$. A relation between the ion energy E and the favorable area $P(A_{\mu\alpha})$, which is dependent on $A_{M\alpha}$, can be assumed from the concepts of the developed sputtering collision theory as follows. It has been assumed that for sputtering collisions at perpendicular ion incidence, the condition $m \ll M$ can be applied for the first collision of the ion with a lower surface atom. With this condition, the compression impulse R_c from Eqs. (3.5) and (3.4) with $V_0 = 0$ is given for an oblique collision by

$$R_c = \delta m v_0 \cos i_\alpha, \quad (7.5)$$

so that the energy involved is

$$R_c^2 / 2m = \delta^2 E \cos^2 i_\alpha, \quad (7.6)$$

if $E = \frac{1}{2} m v_0^2$ is the energy of the impinging ion.

This is also the energy regained during the phase of expansion since $R_e = R_c$. If $\delta = 0$, the whole energy would be dissipated in Debye waves and sputtering could not occur at all. The larger δ , the higher is the energy regained.

Thus, as a reasonable assumption, the area $A_{M\alpha}$ can be set proportional to $\delta^2 E \cos^2 i_\alpha$ with a factor ν^2 of dimensions $[m^2]$ by the equation

$$\nu^2 A_{M\alpha} = E \delta^2 \cos^2 i_\alpha, \quad (7.7)$$

which with the abbreviation

$$q_\alpha = \delta^2 \cos^2 i_\alpha / \nu^2 \quad (7.8)$$

can be written as

$$A_{M\alpha} = q_\alpha E. \quad (7.9)$$

The area $A_{M\alpha}$ is the surface of a spherical segment on the collision sphere c_M of the target atom M_L ; therefore, as seen from Fig. 10,

$$A_{M\alpha} = 2\pi c_M^2 (1 - \cos \epsilon_\alpha) \quad (7.10)$$

and thus from Eqs. (7.8) and (7.9)

$$\sin^2 \epsilon_\alpha = \frac{q_\alpha}{\pi c_M^2} \left(E - \frac{q_\alpha E^2}{4\pi c_M^2} \right). \quad (7.11)$$

If this value is inserted into Eq. (7.3), then the sputtering rate from Eq. (7.1) can be written in the form

$$S_{hkl} = s_{hkl} \left(\frac{E^2 t_{hkl}}{4\pi c_M^2} - E \right), \quad (7.12)$$

where

$$s_{hkl} = \frac{c_\mu^2}{c_M^2 A_{hkl}} \sum_{\alpha}^{a_1, a_2, \dots} p_\alpha q_\alpha \cos i_\alpha \quad (7.13)$$

and

$$t_{hkl} = \frac{\sum_{\alpha}^{a_1, a_2, \dots} p_\alpha q_\alpha^2 \cos i_\alpha}{\sum_{\alpha}^{a_1, a_2, \dots} p_\alpha q_\alpha \cos i_\alpha}. \quad (7.14)$$

For the threshold energy E_{\min} , p_α , i_α , and thus q_α , s_{hkl} , and t_{hkl} can be determined for each low plane of any crystal system, if assumptions are made about δ , c_M , c_μ , and ν^2 . If there is only one α angle in the unit area, t_{hkl} is equal to $q_\alpha = \delta^2 \cos^2 i_\alpha / \nu^2$. Different sputtering rates at the threshold energy can be expected for different single-crystal planes of the same as well as of different crystal systems. The calculation of s_{hkl} and t_{hkl} becomes more complicated for higher ion energies, since sputtering can then also occur by collisions from second or third lower atoms or by triple collisions. In this case the single unit area is no longer representative for the sputtering rate, but several unit areas together must then be considered as a new unit area for the calculation, similar to the case of polycrystalline targets treated below.

Equation (7.12) gives the relation between the sputtering rate S_{hkl} and the ion energy E for an ideal low index plane (hkl) of a single crystal at normal ion incidence. Of course, after sputtering has started, upper surface atoms have been removed and the formerly lower surface atoms are now upper ones. If this happens uniformly over the whole exposed surface, then the factors influencing the sputtering rate such as the angles $\alpha_1, \alpha_2, \dots$, the number of favorable areas $p_{\alpha_1}, p_{\alpha_2}, \dots$ and the incidence angles $i_{\alpha_1}, i_{\alpha_2}, \dots$ within the unit areas A_{hkl} would nevertheless be the same so that the Eq. (7.12) would remain applicable. That such a behavior is very probable can be concluded from the following experimental facts. If in spot pattern experiments^{3,12} the small spot of a single-crystal plane is first sputtered near the threshold energy, a distinct pattern characteristic for the lowest ion energy is obtained at a certain sputtering rate. If now the ion energy is increased to a value three or four times the threshold energy, the sputtering rate will be higher and the resulting spot pattern changed considerably, due to the fact that other directions α_n from second or third lower atoms to upper surface atoms are now effective. The surprising fact now is, as observed by Wehner, that the threshold pattern is again obtained from this surface, which is no longer ideal, if the target is again submitted to sputtering at the lowest ion energy, and the sputtering rate is the same as before.

7.4. Sputtering Rate Equation for Polycrystalline Targets at Low Ion Energies

In polycrystalline targets the total area exposed to sputtering can be represented by $\sum_{hkl} n_{hkl} A_{hkl}$, where the summation has to be extended over all the low-index planes (hkl) present in the surface plane of the target, and n_{hkl} are the numbers of the corresponding unit areas A_{hkl} . Then the sputtering rate can be considered as the average

$$S = \frac{\sum_{hkl} n_{hkl} A_{hkl} S_{hkl}}{\sum_{hkl} n_{hkl} A_{hkl}}, \quad (7.15)$$

with S_{hkl} from Eqs. (7.12), (7.13), and (7.14). If the abbreviations

$$s = \frac{\sum_{hkl} n_{hkl} A_{hkl} S_{hkl}}{\sum_{hkl} n_{hkl} A_{hkl}}, \quad (7.16)$$

$$t = \frac{\sum_{hkl} n_{hkl} A_{hkl} t_{hkl}}{\sum_{hkl} n_{hkl} A_{hkl}}, \quad (7.17)$$

are used, then Eq. (7.15) for polycrystalline targets can be written in the form

$$S = s \left(\frac{E^2 t}{4\pi c M^2} - E \right). \quad (7.18)$$

In this equation s and t , since dependent on S_{hkl} and t_{hkl} , are not really constant, but, as explained above in discussion of Eqs. (7.13) and (7.14), s and t may be in a certain degree different for higher and lower ion energies. S in Eq. (7.18) is submitted to the condition, that the lowest value S_{\min} is obtained for the threshold energy E_{\min} , thus

$$S_{\min} = s \left(\frac{E_{\min}^2 t}{4\pi c M^2} - E_{\min} \right). \quad (7.19)$$

For values of $E < E_{\min}$ there is no sputtering; thus $S=0$. If the differences of s and t for different energies are disregarded, then the minimum condition (7.19) can be combined with Eq. (7.18) by writing

$$S - S_{\min} = s \left\{ \frac{t}{4\pi c M^2} (E^2 - E_{\min}^2) - (E - E_{\min}) \right\}. \quad (7.20)$$

The minimum condition, $dS/dE=0$, $d^2S/dE^2 > 0$ from Eq. (7.18) yields the value

$$E_{\min} = 2\pi c M^2 / t \quad (7.21)$$

so that if this value is inserted into Eq. (7.20) and if ϕ is introduced by the equation

$$\phi = E_{\min} / s, \quad (7.22)$$

then the sputtering-rate equation (7.20) becomes

$$S - S_{\min} = (E - E_{\min})^2 / 2\phi \quad (7.23)$$

which holds for $E \geq E_{\min}$, while $S=0$ for $E < E_{\min}$.

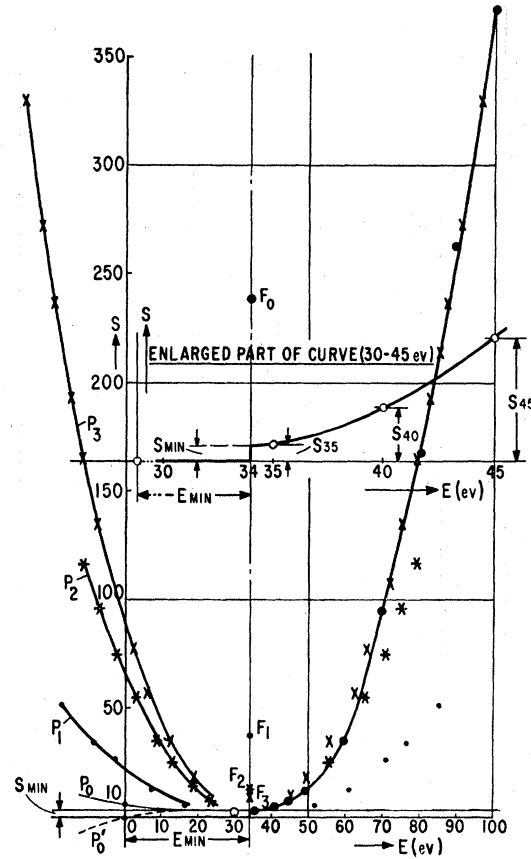


FIG. 11. The sputtering rate S versus ion energy E for Pt-Xe replotted from Wehner and Medicus¹³ (with S instead of \sqrt{S}) and compared with four parabolas of different parameters ϕ , demonstrating the variation of the parameter ϕ in the sputtering rate law: $S - S_{\min} = (E - E_{\min})^2 / 2\phi$ for $E \geq E_{\min}$; $S=0$ for $E < E_{\min}$.

The curve of the sputtering rate S vs E from Eq. (7.23) with these conditions can be recognized as one branch of a parabola with the vertex at $S=S_{\min}$ and $E=E_{\min}$, if ϕ is considered as the parameter of the parabola. But, as emphasized, s is dependent on the energy E and has the smallest value for the threshold energy; thus the parameter ϕ also varies with the energy and has the largest value near the threshold energy.

7.5. Comparison with Experimental Data

The only reliable curves of the sputtering rate S vs E at low ion energy, known from literature, are the curves for Pt with Xe ions¹³ and for Pt with Hg ions.⁴ The Pt-Xe curve is replotted in Fig. 11, on the right side, with values of S instead of \sqrt{S} , while on the left side of the same figure four parabolas with the same vertex but with different parameters are drawn. The lower part of the S curve between 34 eV, which is the threshold energy, and 45 eV fits the parabolas P_0 and P_1 best (except the first experimental point, which has been disregarded). The upper part of the curve between 70

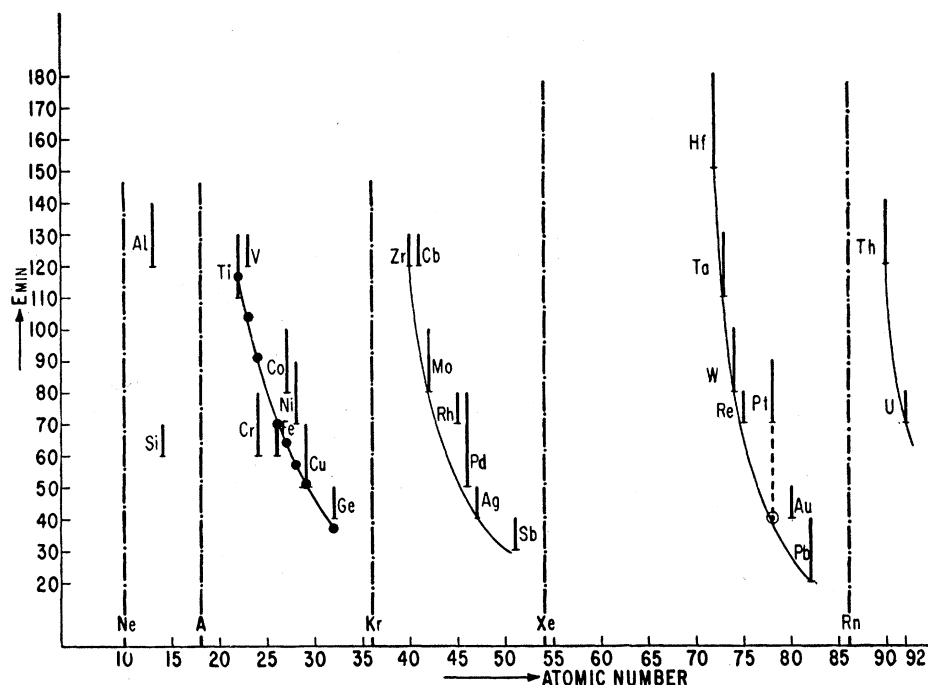


FIG. 12. Periodicity of the threshold energies E_{min} of 26 different metals with Hg ions, as determined by Wehner,² in a plot *vs* atomic number. The encircled value $E_{min}=40$ ev for Pt was measured by Wehner and Medicus¹³ with Xe ions.

and 100 ev (and as checked, but not represented up to 200 ev) perfectly fits the parabola with the smallest parameter (focal point F_3).

7.6. Extrapolation of the Threshold Energies from Experimental Curves S vs E

The practical value of the knowledge of the sputtering rate law lies in the fact that time consuming measurements of the sputtering rate at the lowest ion energies near threshold can be avoided. As seen from Fig. 11 the curve S vs E can be approximated in its different parts by parabolas having different parameters, but the same axis. For each part of the curve between energy values E_1 and E_2 for which the slope of the curve is noticeably different, the focus of the approximating parabola can be determined by a simple well-known geometrical construction. If two or more such energy intervals of the curve are chosen, and the foci of the approximating parabolas are geometrically determined, then all the foci should have the same abscissa. In case of small deviations a mean value of these abscissas can be considered as threshold energy E_{min} .

8. PERIODICITY OF THRESHOLD ENERGIES

From the sputtering-rate formula derived above, an interesting conclusion can be made about the relation between the threshold energy and the assumed collision radius of the target atom. Equation (7.21) resulted as the ion energy for which the sputtering rate S has the minimum value, where c_M is the collision radius for the target atom, while t for polycrystalline targets is given by Eq. (7.17) and the value of t for a distinct single

crystal plane with only one α angle reduces to

$$t = \delta^2 \cos^2 i_\alpha / v^2 \quad (8.1)$$

as explained in detail under (7.8). Since v^2 , as defined by (7.5), is assumed to be a constant, and the coefficient of dissipation δ is approximately the same for different target atoms of the same crystal system sputtered with the same ions, the value of t at threshold energies is determined by the incidence angles i_α . However, these angles are determined by the crystal planes and the crystal system only, so that t is the same for different target materials of the same crystal system, and of the same order of magnitude for targets of other crystal systems.

From these considerations, one can expect from Eq. (7.21) that the threshold energies for different metals sputtered with the same kind of ions are roughly proportional to the square of the collision radii c_M of the target atoms.

Since the sizes of the effective radii of the largest closed shells of the target are different for the elements according to their atomic number, a relation between the threshold energies and the collision radii c_M in the derived form (7.21) should already be coarsely visible in a plot of the threshold energies of the different elements *versus* atomic number.

The threshold energies of 26 metals with Hg ions, determined by Wehner,² are plotted in Fig. 12 in this manner, and one can immediately see from this plot that the threshold energies of the elements between the noble gases follow a certain law. This law requires, within each period, higher threshold energies for the elements with the lower atomic numbers.

It now remains to be checked as to whether the derived relation (7.21) with tentatively assumed collision radii is able to cover this law in a satisfying manner.

An estimation of the collision radii c_M of the largest closed electronic shells can be obtained from data on the radii of electronic orbits, tabulated by Slater¹⁴ for the lighter elements, and from data on the radii R associated with hard-sphere collisions of knocked-on atoms in the theory of radiation damage.⁸ The radii of electronic orbits represent the distance from the nucleus at which the radial charge density (the charge contained in a shell of unit thickness) is a maximum. These radii are tabulated in Table II for the M shells of elements of the fourth period, for which the threshold energies have been determined by Wehner.² A weighted average value r_m of these orbits is determined by the relation

$$r_m = (2r_{M3s} + 6r_{M3p} + dr_{M3d}) / (8 + d), \quad (8.2)$$

where d is the number of electrons in the subshell $M3d$. The effective collision radius c_M of the largest closed shell is assumed to be a multiple of r_m , which can be estimated from data on copper discussed in the theory of radiation damage. In this theory the radius R associated with hard-sphere collisions of knocked-on atoms and the mean free path L_s of these atoms, connected with R by the relation $L_s = \frac{4}{3}r_s^3/R^2$, where r_s is the atomic radius, are dependent on the energy of the knocked-on atom. If this energy is 300 ev, then the most probable value from the theory of radiation damage is $L_s = 5r_s$. Since the energy of the impinging ion, which is comparable to the energy acquired by the knocked-on atom is considerably lower for the threshold energies which are between 40 and 150 ev, a mean value of $L_s = 2.7r_s$ seems to be a reasonable assumption.

In this case the radius R would be $R = 0.7r_s$; thus for copper $R = c_M = 0.89$ A since $r_s = 1.27$ A, while the value $c_M = 0.68$ A, as used above in Fig. 2 in Sec. 4.1 corresponds to the value of $L_s = 4.65r_s$ to somewhat higher energies. If c_M for copper is chosen as 0.89 A, then the multiplying factor for $r_m = 0.33$ A is 2.7. This value has been used in Table II for all the elements. The square of c_M multiplied with an arbitrary factor gives values very close to the threshold energies, measured by Wehner.²

The calculated values of c_M^2 multiplied by an arbitrary factor (which is chosen to be 64 in Table II) are drawn in the plot of Fig. 12 as circles, and are connected by a curve. Similar curves are drawn in the other periods between the lowest values of the threshold energies which, as explained above, are considered to be closer to the real threshold energies.

The values of some elements deviate from these curves; for instance, Cr deviates to the lower side and Pt to the higher side. The low value for Cr can probably

TABLE II. Proportionality of the threshold energies E_{\min} to the squares of the tentatively calculated collision radii c_M of the largest closed electronic shells of elements of the fourth period of the periodic system.^a

Atomic number	Element	r_{M3s} (A)	r_{M3p} (A)	r_{M3d} (A)	r_m (A)	$\frac{c_M}{2.7r_m}$ (A)	$c_M^2 \times 64$	E_{\min} (ev)
22	Ti	0.48	0.50	0.55	0.50	1.35	117	110-130
23	V	0.46	0.47	0.49	0.47	1.27	104	120-130
24	Cr	0.43	0.44	0.45	0.44	1.19	91	60-80
26	Fe	0.39	0.39	0.39	0.39	1.05	70	60-70
27	Co	0.37	0.37	0.36	0.37	1.00	64	80-100
28	Ni	0.35	0.36	0.34	0.35	0.94	57	70-90
29	Cu	0.34	0.34	0.32	0.33	0.89	51	50-70
32	Ge	0.30	0.30	0.27	0.28	0.76	37	40-50

^a r_{M3s} , r_{M3p} , r_{M3d} = radii of electronic orbits in the $M3s$, $M3p$, and $M3d$ shell, representing the distance from the nucleus, at which the radial charge density (the charge contained in a shell of unit thickness) is a maximum (see reference 14). $r_m = (2r_{M3s} + 6r_{M3p} + dr_{M3d}) / (8 + d)$, where d = number of electrons in $M3d$ shell. E_{\min} = threshold energy at normal ion incidence with Hg-ions (see reference 2).

be explained by the fact that because of the lack of Cr sheet metal, the experiments were made with a chromium surface produced by electrodeposition, which very probably requires only a considerably lower energy to start sputtering. The high value of the threshold energy for Pt (70 to 90 ev) with Hg ions from the table of Wehner² has already been discussed in connection with the sputtering rate. The threshold energy for Pt with Xe ions was found by Wehner and Medicus¹³ to be 40 ev and was calculated as 35 ev from the sputtering-rate curve above. From the threshold formula (5.11) and the plot of the function $g(m, M)$ in Fig. 6, one can expect that the value of the threshold for Pt with Hg ions is not much different from the value of Pt with Xe ions, provided that the influence of the coefficient of dissipation δ is negligible. With the threshold energy of 35 to 40 ev, as seen from Fig. 12, Pt fits the curve in the sixth period from Pb to Hf very well.

It remains to be investigated whether other minor discrepancies, for instance, the higher values for Co and Ni in the iron triad FeCoNi and for Rh and Pd in the triad RuRhPd, have a physical meaning or are due to experimental indetermination. More refined measurements of the threshold energies are certainly necessary, before further conclusions can be drawn from these deviations.

ACKNOWLEDGMENTS

The work was initiated while assisting the experimental work on sputtering of Dr. G. Wehner¹⁵ of this Laboratory with microscope, electron-microscope, and x-ray diffraction work, and studying the results of his investigations. It was encouraged in the basic concepts by Dr. G. Medicus. The author is grateful to Major H. Triwush, Dr. J. W. Ballard, and T/Sgt. S. Derby for valuable assistance in preparing the manuscript.

¹⁴ J. C. Slater, *Introduction to Chemical Physics* (McGraw-Hill Book Company, Inc., New York, 1936), p. 349.

¹⁵ Now with General Mills, Inc., Mechanical Division, Minneapolis, Minnesota.